

# A Parametric Approach for the Geocoding of Airborne Visible/Infrared Imaging Spectrometer (AVIRIS) Data in Rugged Terrain

Meyer Peter

Jet Propulsion Laboratory, California Institute of Technology  
4800 oak Grove Drive Pasadena, CA 91109, pmeyer@rsl.geogr.unizh.ch<sup>1</sup>

## ABSTRACT

*A geocoding procedure for remotely sensed data of airborne system in rugged terrain is affected by several factors: buffeting of the aircraft by turbulences, variations in ground speed, changes in altitude, attitude variations, and surface topography. The current investigation was carried out in Central Switzerland, using two Airborne Visible/Infrared imaging Spectrometer (AVIRIS) scenes out of NASA's Multi Aircraft Campaign (MAC) in Europe (1991). The first scene was acquired over flat and hilly terrain and the second over a mountainous area with steep slopes. The parametric approach reconstructs for every pixel the observation geometry based on the flight line, aircraft attitude, and surface topography. Aircraft navigation data, instrument engineering data, information from a conical radar tracking system, and a digital elevation model are used. To prevent changes to the radiometric characteristics, the original value is selected by an improved extraction algorithm, thereby eliminating the need to interpolate the values. The results are visually checked for correspondence at locations with different slope and aspect angles by overlaying scanned forest maps and digitized shorelines of the Swiss Topographical Map. This validation is completed by a quantization of the spatial deviation at selected points and a comparison with an improved non-parametric approach. In general the results show very good correspondence with the maps. The algorithm reported in this article is a necessary base to apply georadiometric correction methods for slope - aspect dependent illumination corrections, atmospheric corrections, and to use AVIRIS data within single-pixel based information systems for land use classification.*

## INTRODUCTION

Remotely sensed data have geometric characteristics and representation which depend on the

---

<sup>1</sup> now at: University of Zurich-Itzehel, Remote Sensing Laboratories, Winterthurerstrasse 190, CH-8057 Zurich

type of acquisition system used. To correlate such data over large regions with other real world representation tools like conventional maps or Geographic Information Systems (GIS) for verification purposes, or for further treatment within different data sets, a coregistration has to be performed. To correct for slope and aspect effects in a radiometric sense, for example, the exact location of a pixel is required (Itten and Meyer, 1993).

in addition to the geometric characteristics of the sensor there are two other dominating factors which affect the geometry: the stability of the platform and the topography. For aircraft instabilities, the flight line ( $x, y, z$ ) and the attitude (roll, pitch, true heading) will cause shear, splay, compression and expansion of the image. Airborne sensors normally have wide Fields of View (FOV) of  $> 20^\circ$ , which result in a panoramic distortion of the data. Topography influences the geometric quality by shifting the recorded pixel location compared with the true position, and by affecting the pixel size.

There are two basic approaches for a geometric correction on a pixel-by-pixel basis: (a) A parametric approach using the location of the airplane and inertial navigation system data to simulate the observation geometry and (b) a non-parametric approach using tie points or ground control points. In the non-parametric approach good distinguishable landmarks in the image are selected and compared with the corresponding points in the reference system. Very often, this selection process turns out to be very time intensive. It is well known that the non-parametric approach is not reliable enough for the unstable flight conditions of airborne systems, and is not satisfying in areas with significant topography, e.g. mountains and hills. An improved version of the basic non-parametric approach, combined with a shift-correction was presented for Landsat Thematic Mapper (TM) data in Itten and Meyer (1993).

A parametric approach was published by Guindon (1980) for the integration of MSS and SAR data and by Frey et al. (1989). They are assuming a constant flight altitude, flight path as a straight line (acquired out of calculation with ground control points), no attitude changes and a constant true airspeed. Frey et al. achieved within their case study for an airborne Bendix M2S Scanner and a digital elevation model (DEM) of 5m grid size a standard deviation of  $\pm 2.6$  pixels and  $\pm 2.4$  pixels for  $x$  and  $y$  direction respectively for a maximum elevation difference of 250m. Kalcic and Lingsch (1991) correct the attitude movements and scan angle distortion of the scanner of the Naval Oceanographic and Atmospheric Research Laboratory (NOARI) for the Airborne Bathymetric Survey. The result

shows a root mean square (RMS) error of 25.7m over a flat urban test site.

The present work describes a parametric preprocessing procedure which corrects effects of flight line and attitude variation as well as topographic influences. The study has been carried out using Airborne Visible/Infrared Imaging Spectrometer (AVIRIS) data (Vane et al., 1993). It is part of the geometric preprocessing module of the Information Management System for Remote Sensing (IPRS) as reported by Meyer (1992) and Meyer and Itten (1992). The IPRS approach proposes two parts, information extraction and information management, to complete processing of remotely sensed data. The first part consists of the modules data quality assessment and preprocessing and the latter of the modules classification and presentation.

## **BASIS OF THE STUDY**

### **Test site**

The area "Zug-Buochserhorn" is the standard test site of the Remote Sensing Laboratories, University of Zurich-Itchen, for investigations using different sensors and for differing applications. This site is about 20km south of Zurich (Itten and Meyer, 1993; Meyer et al., 1993a). The region covered by the AVIRIS flight #910705, run 6 of the NASA MAC Europe '91 campaign is split into three different scenes of about 11 km x 9 km (Itten et al., 1992). The first two scenes have been selected for the current investigation: the first, Zug, represents a hilly region which is dominated by Lake Zug and the surrounding hills with highest elevation difference of about 600m and slopes with typical angles between 15° and 60°. This area, composed of molassic segments, contains agricultural fields and forest stands. The second scene, Rigi, is an example of mountainous terrain. This region is dominated by the Rigi mountains which represent the border between the Central Plateau's molassic sediments and alpine Helvetian layer. The elevation difference is about 1400m and results in steep slopes. The lower territories are primarily covered by coniferous (mainly *Pinus abies* and *Abies alba*) and deciduous (mainly *Fagus sylvatica*) stands. The higher elevations are bare slopes with rocks. The maximum slope angle for this area is 90°.

### **AVIRIS auxiliary data**

The geometric, radiometric, and spectral quality assessment for the actual data set as well as the

sensor, system and scene specific influences are described in detail in Meyer et al. (1993b). The current work uses the navigation data roll, pitch, and true heading (which is the pointing direction of nose of the aircraft). These are generated through the ER-2 Inertial Navigation System and the Air Data Computer. From the AVIRIS instrument's precision gyros, roll and pitch are used. The raw data needs to be processed prior to use. All auxiliary data generated by the instrument's rate gyros are affected by the earth's rotation (Litton System Inc., 1989; Genofsky, 1986; The Singer Company, 1984). The roll rate error  $ER$  and the pitch rate error  $EP$  (in deg/min) due to earth rotation are calculated on a line-by-line basis using Equation (1) and Equation (2) as follows:

$$ER = (\cos \theta_l) (\cos \theta_p) KE, \text{ and} \quad (1)$$

$$EP = (\cos \theta_l) (\sin \theta_p) KE, \quad (2)$$

where  $KE$  = Earth's rotation rate ( $0.25^\circ/\text{min}$ ),  $\theta_l$  = aircraft latitude ( $0^\circ$  at equator,  $+90^\circ$  at north pole), and  $\theta_p$  = aircraft flight direction ( $0^\circ$  flying true north,  $+90^\circ$  true east). The true heading value from the navigation data is already corrected for Earth rotation by the navigation system.

#### *Pitch information*

The engineering data provides eleven pitch readings for every scan line. A cubic spline interpolation is used to generate a pitch value for every pixel of a line to account for movements of the plane within a scan line. However, as described in a detailed quality assessment (Meyer et al., 1993b), spikes in the original 11 readings make it advisable for this data set to use only the first reading as representative for the line. When the pilot turns on the mechanism the AVIRIS gyros are set equal to 0. Sometimes, due to aeronautical reasons, the ER-2 is not fully levelled at this time. Since the current procedure requires the better resolution of the engineering gyro, the offset has to be determined using the value of the navigation pitch at line #1. The total pitch value is calculated using the pitch value of the first reading and the pitch offset.

#### *Roll information*

The engineering roll data is used to verify that the roll movement was within the range of the roll compensation of  $\pm 1.5^\circ$ . This is necessary, because the instrument gyro loses its zero position after being saturated. The roll offset is defined by averaging the navigation roll value every time the engineering roll gyro hits the 0-line. However, additional investigations show that the difference in the sensitivity of the gyros for these rapidly changing roll movements make it necessary to optimize

the value using landmark calculations.

### *True heading information*

The AVIRIS instrument's gyros do not supply true heading information. To determine the heading direction of the plane, the true heading information of the ER-2 gyro has to be used, despite the low update rate of 5 seconds. Aeronautical considerations suggest that such movements are performed more slowly than around the other axes and the induced error should be negligible. The navigation gyro uses magnetic north as a reference point. Since all ground reference information such as maps and digital elevation models (DEM) use geographic north (meridian convergence), the declination has to be corrected. The declination was 0.019780rad (Zug), and 0.019199rad (Rigi) for the two test sites in July 1991.

### **AVIRIS image data**

Two runs were recorded over the Zug-Buochserhorn test site during the MAC Europe'91 campaign on July 5, 1991. Run 6 was flown at 12:08 GMT from north to south, resulting in three scenes with an average nominal pixel size of about 18m. For this run there are no Daedalus ATM1268 scanner data or RC-10 aerial photographs available. The four scenes for run 7 were acquired flying from south to north immediately after run 6. Due to the instrument's roll gyro saturation, the data from run 7 can not be used for the current investigation (Meyer et al., 1993 b).

### **Digital elevation model**

The test area is covered by the three digital models (DHM-25) Zug, Rigi, Beckenried. They are generated and distributed by the Swiss Federal Office of Topography and have a resolution of 25m in x and y direction and of 0.10 m in elevation z (Rickenbacher, 1992). The average error in elevation is  $2.2\text{m} \pm 1.0\text{m}$  for model Zug, and  $4.4\text{m} \pm 1.8\text{m}$  for Rigi. The original grid size of 25m has been resampled to 6m and 18m for this study using a bilinear interpolation algorithm.

### **ADOUR conical radar tracking system**

#### *Short description*

The ground-based immobile tracking radar system ADOUR is a dual antenna, dual frequency radar with a conical scan tracking system operated by the Swiss Air Force (Horn et al., 1993; Thom-

son-CSI, 1987). The results of these two devices are independent. The system provides different parameters. For the current approach the latitude  $x$ , longitude  $y$ , and altitude  $z$  are used. The information is transformed in the standard Swiss Military Coordinate System, which is used for the topographic maps, too. The systematic error for elevation and azimuth is  $\pm 0.2$  mrad and  $\pm 7$  m for a distance with an update interval of 0.2 second. The distance between the system and the flying target is between 36 km and 68 km.

### *Accuracy assessment*

As mentioned above, there are no RC-10 aerial photographs available for run 6. Therefore, to get an idea about the accuracy of the system the data from run 7 are used. The validation of the ADOUR data was carried out in two steps. The first step checks the relative stability between the two devices for the full run 7. The values shown in Table 1 (upper line) are for a total tracking distance of 34,959 m. The next step determines the absolute accuracy. The idea is to compare the projection center of the RC-10 aerial photograph with the corresponding ADOUR data. These points are determined, using a one-step approach based on collinearity on a Wild AC-3 analytical plotter at the Institute of Geodesy and Photogrammetry of the Swiss Federal Institute of Technology. The best way to correlate the two sources would be to use time correspondence. Unfortunately, the time information of the RC-10 frame information is not accurate enough, compared with the resolution of the ADOUR system that has 5 measurements each second. The ADOUR clock is permanently double-checked with time reference pulses from an atomic clock, type DCF77WA31 with an absolute mean error of  $10 \text{ ms} \pm 5 \text{ ms}$ . The correlation has to be established by defining the nearest neighbor in  $x$  and  $y$  direction of the projection centers to the ADOUR values, despite uncertainties of the time correspondence. The value for the altitude  $z$  of Table 1 (lower line) is, due to the local stability of the aircraft, independent of the quality of the correspondences and demonstrates the performance of the system. The significantly better values for the  $y$  direction result from the overlaying process on the flight line, which was straight south-north. There is no correction applied to allow for the distance between the nose bay, where the RC-10 camera is located, and the E bay, where AVIRIS is carried. Further analysis shows that there is a correlation between the distance of the target to the device and the accuracy. Figure 1 shows the regression for the comparison between the altitude of the projection center of the RC-10 and the corresponding ADOUR data for a correlation with an  $r^2$  of 0.78. There is a maximum deviation of 12 m over the full run of 32,000 m, which satisfies the system requirements (See "Short description"). Errors resulting from refraction at the different atmospheric layers should be negligible.

due to the high elevation angle for the current geographical situation.

### *Preparation*

The sampling rate of the ADOUR system dots not correspond with the number of lines per scene. Therefore, the data are resampled to 6m intervals using a cubic spline interpolation. To avoid margin errors, the required number of lines are selected out of the entire flight line.

## **Ground reference information**

### *Forest map*

The forest map was generated by scanning the green (forest) plate of the Swiss Topographic Map, scale 1:25,000, edition 1987 at 50  $\mu\text{m}$  with the Optronics 5040 Scanner of the Swiss Federal Institute of Technology, Department of Cartography. The data were vectorized on an Intergraph System MicroStation 4 and resampled to 18m grid size on a Aries-111 Dipix System. The average cartographic accuracy is about 5.0m. The average location error for a photogrammetric analysis for the forest border is 1.0-2.0m. Compact forests are represented with a surrounding solid boundary line. If the boundary between the forest and non-forest is poorly defined, as it is around the timber line or in the neighborhood of swamps, a symbolic point signature was used. However, this signature was suppressed during the preparation process of the map.

### *Shoreline map*

The map was produced by digitizing the Swiss Topographic Map, scale 1:25,000, edition 1987 in an ARC/info using a digitizing tablet. The average (theoretical) accuracy is  $\pm 8.0\text{m}$  using an average sea level to determine the shoreline.

## **METHOD**

Figure 2 gives an overview of the core task for the new method for geocoding AVIRIS data. The basic goal is to reconstruct for every pixel the geometric situation at the time it was acquired with AVIRIS. This includes three major aspects. The first considers the flight line and attitude of the ER-2 aircraft, the second the current observation geometry and the third the situation on the surface. This approach includes three different coordinate systems: the raw file, containing the recorded pixels at location (c,r) where c is the column and r the row number; the observation geometry, which is

described by longitude  $x$ , latitude  $y$ , and altitude  $z$  of the airplane together with roll  $\omega$ , pitch  $\phi$ , and true heading  $\chi$ ; the DEM coordinates  $(i,j)$  with elevation  $e_i, j$ . The raw file uses pixels as an entity. The observation geometry and the DEM coordinates are based on the standard Swiss Military Coordinate System.

### Flight line and attitude of the ER-2 aircraft

The latitude, longitude, and altitude of the aircraft needs to be known as a first step. For the 1991 European flights, the  $x, y$ , and  $z$  information results from an unaided LTN90-116 INS navigation system with a position accuracy of 0.9 nautical miles per hour (Perrin, 1993). The navigation data of AVIRIS were updated only every 5 seconds (every 60 lines) and digitized to 8-bits. This data are not accurate enough for the current approach. Therefore, ADOUR data are used as an alternative. The  $x, y$ , and  $z$  measurements consider ground speed variations of the ER-2 aircraft. The description of the attitude of the aircraft is based on the true heading from the navigation data and the roll offset and total pitch of the engineering data (See chapter "BASIS OF THE STUDY").

### Current observation geometry

The basic idea is shown in Figure 3 and described in more detail by Larson et al. (1994). The effort is to observe the underlying surface out of the well-known location (= flight line) and the current attitude of the aircraft. Figure 3 shows the general situation before topography is taken into account. The position vector  $X_{c,r}$  [Eq. (3)] represents the location of pixel  $(c,r)$  in the aircraft coordinate system  $(x,y,z)$  at the instant the pixel was acquired by the instrument. Since the aircraft is moving relative to the image coordinates  $(c,r)$  it is necessary to compute this vector separately for each pixel.  $X_{c,r}$  represents the location of pixel  $(c,r)$  in the ideal case where  $\omega = \phi = \chi = 00$ .

$$X_{c,r} = \begin{pmatrix} 0 \\ \left\{ \tan \left[ (c - \text{is\_flux} - 1) \cdot \frac{FOV}{maxP} \right] z_{x,y} \right\} z_{x,y} \\ z_{x,y} \end{pmatrix}, \quad (3)$$

where  $c$  = pixel number of pixel  $(c,r)$  within line  $r$  of raw image,  $maxP$  = maximum number of pixels per line (614),  $FOV$  = Field of View (in rad), and  $z_{x,y}$  = altitude of ER-2 for the current longitude and latitude (in m).

The pixelwise calculation of the actual pointing direction includes correction of the panoramic

distortion. The vector  $X_{c,r}$  is modified by rotations about the pitch, roll and true heading axis (vector  $X_{c,r}'''$  in Fig. 3). The exact transformation is computationally expensive, and can be replaced by the first-order approximation [Eq. (4)]:

$$\begin{pmatrix} \cos\chi & -\sin\chi & 0 \\ \sin\chi & \cos\chi & 0 \\ 0 & 0 & 1 \end{pmatrix} \begin{pmatrix} \cos\phi & 0 & -\sin\phi \\ 0 & 1 & 0 \\ \sin\phi & 0 & \cos\phi \end{pmatrix} \parallel \begin{pmatrix} 1 & 0 & 0 \\ 0 & \cos\omega & -\sin\omega \\ 0 & \sin\omega & \cos\omega \end{pmatrix} \cong \begin{pmatrix} 1 & -\chi & -\phi \\ \chi & 1 & -\omega \\ \phi & \omega & 1 \end{pmatrix}. \quad (4)$$

The linearized transformation is independent of the order in which the rotations are taken. The transformed position vector  $X_{c,r}'''$  is computed with Equation (5) as follows:

$$X_{c,r}''' = \begin{pmatrix} 1 & -\chi & -\phi \\ \chi & 1 & -\omega \\ \phi & \omega & 1 \end{pmatrix} X_{c,r}. \quad (5)$$

The resulting vector  $X_{c,r}'''$  points now in the direction AVIRIS was “looking” at the time pixel (c,r) was recorded and stored at position (c,r) in the raw file. In preparation for the next step it is necessary to express the transformed pixel location vector  $X_{c,r}'''$  in the DEM coordinate system (i,j). This is accomplished by scaling  $X_{c,r}'''$  by the reciprocal of the DEM horizontal resolution  $\upsilon$  which is for the current investigation equal 6m:

$$X_{i,j}''' = \frac{1}{\upsilon} X_{c,r}''' \quad (6)$$

### Situation on surface

The topography causes a shift in the apparent pixel location, and affects the pixel size. The idea of the pixel location vector allows for compensation of both effects within one step.

#### *True nadir for the first line*

The nadir is supposed to be at the position “half of the maximum number of pixels per line”. Due to the presence of a roll offset, the true nadir position has to be defined using Equation (5) with  $c=307$  and line  $r=1$  and the ADOUR values.

### Intersection with surface

The goal is now to find the intersection between the pixel location vector  $X_{i,j}'''$  and the surface of the DEM. Within the neighborhood around the transformed pixel location vector  $X_{i,j}'''$ , a test vector  $X_{i,j}^*$  is searched for, which converges to  $X_{i,j}'''$ .

$$X_{i,j}^* = \begin{pmatrix} i - i_{Nadir} \\ j - j_{Nadir} \\ (z_{x,y} - e_{i,j}) \\ v \end{pmatrix}, \quad (7)$$

where  $i_{Nadir}$  = i-coordinate of true nadir point,  $j_{Nadir}$  = j-coordinate of true nadir point,  $e_{i,j}$  = elevation of test point at position (i,j), and  $z_{x,y}$  = altitude of ER-2 for the current longitude and latitude. To allow for a more precise selection of the corresponding surface point, the DEM oversampled to a grid size of 6m is used (See chapter "BASIS OF THE STUDY").

To define the intersection point on surface, the normalized dot product DP is calculated:

$$DP = \left( \frac{X_{i,j}^* X_{i,j}'''}{|X_{i,j}^*| |X_{i,j}'''} \right). \quad (8)$$

The vector  $X_{i,j}^*$  best representing  $X_{i,j}'''$  is that for which the dot product DP has the smallest difference from 1. Vector components  $xX_{i,j}^*$  and  $yX_{i,j}^*$  together with the altitude  $zX_{i,j}^*$  of the best fitted vector represent the surface point (i,j) of the DEM.

To determine the first test point for each scan line, a new line is constructed with the Bresenham line algorithm (Ferraro, 1988). The starting point of this line is the true nadir point, the end point is determined as the intersection of  $X_{i,j}'''$  with sea level (Fig. 4). For computational efficiency, the test points for the pixels (c,r) with  $c > 1$  are determined through construction of possible test vectors  $X_{i,j}^*$  within a neighborhood of the previously determined best test vector  $X_{i,j}^*$  (Fig. 5).

### Topography dependent pixel size representation

The next step is to separately calculate the four corner points for every pixel. This approach allows the adaptation of the current pixel to the terrain and results in a better estimation of the true pixel size. Therefore, the calculation of the pixel position vector  $X_{i,j}'''$  is updated (compare Eq. (3)):

$$X_{c,r} = \begin{pmatrix} \langle \tan \left\{ \left[ \left( c - \frac{\text{max}P - 1}{2} \right) \frac{\text{FOV}}{\text{max}P} \right] - \text{SHIFT}_{\text{IFOV}_c} \right\} z_{x,y} \rangle \\ z_{x,y} \end{pmatrix}, \quad (9)$$

where  $\text{SHIFT}_{\text{IFOV}_d}$  = down-track shift, which iterates for the four corners with an instantaneous field of view (IFOV) of  $d=0.0009$  rad, and  $\text{SHIFT}_{\text{IFOV}_c}$  = cross-track shift, which iterates for the four corners with an  $\text{IFOV}_c=0.001$  rad, representing corner 1 =  $(\text{IFOV}_c/2, -\text{IFOV}_d/2)$ , corner 2 =  $(-\text{IFOV}_c/2, -\text{IFOV}_d/2)$ , corner 3 =  $(-\text{IFOV}_c/2, \text{IFOV}_d/2)$ , and corner 4 =  $(\text{IFOV}_c/2, \text{IFOV}_d/2)$ .

The ideal vector  $X_{i,j}'''$  is now calculated four times for every pixel (c,r) of the raw file iterating the  $\text{SHIFT}_{\text{IFOV}_d}$  and  $\text{SHIFT}_{\text{IFOV}_c}$ . After the transformation and determination of the best test vector (as described above) the four corner points of every pixel (c,r) are found. These now define a pixel. To determine the included area, a polygon fill algorithm (POLYFILLV; Reseach System Inc., 1993) is used. After this step, every 6m pixel (i,j) points to the corresponding coordinates of 18m pixel (c,r) of the raw image.

### Resampling

Within the final step, the 6m grid size pixel needs to be resampled to the 18m original pixel size. Major effort must be spent to keep the original digital value (DN) from the raw file. This step determines for every one of the resampled 18m pixels, which 6m pixels constitute the new 18m pixel (Fig. 6). The most frequent 6m pixel is selected and using its pointer to address the corresponding pixel (c,r) of the raw image to get its DN value. If within one 18m pixel there are three equal groups, the one with the lowest value is selected. This selection step is repeated for all 224 bands. The process does not change the original DN value and therefore, an additional mixing can be avoided.

## DISCUSSION

There are currently no well-established methods of quantitatively assessing the success of a geocoding process. Visual inspection provides useful information, but cannot be used to intercompare methods. Statistical results based on residual calculation of single ground control points allow only a local error assessment (Frey et al., 1989). The quantitative approach used here is an extension to the ground control point method. Both qualitative and quantitative methods have been used and results

are presented in the discussion along with a comparison with the results of an improved non-parametric approach.

### *Visual verification*

For the discussion, the scene Rigi is selected because of the more challenging topography (Fig. 7, Fig. 8). Nevertheless, this scene includes some flat terrain to demonstrate the performance in such areas as well. Bands 13, 18, and 28 of the geocoded image are overlaid by the scanned forested areas (green line) and digitized shoreline (blue line). The scanned forest border is the only information which is available in every part of the scene and for the most elevations as well as for most varied slope and aspect angles. Part (A) shows the composed image rendered on the DEM25 using the shading function SHADE\_SURF (Research System Inc., ] 993). An observation point which is located 500 above the j-axis of the DEM is chosen for demonstration purpose. Figure 9 gives an impression of the topography along the north-south and east-west cross-section. For the northern part, an azimuth of  $0^\circ$  was selected and for the southern part one of  $180^\circ$ . The characters (B-E) show the topographical locations of the zoom-up subareas of the lower part of the Figure 7 and 8. The enlarged areas (zoom factor  $\approx 5$ ) are selected dependent on their aspect and slope angle to allow verification of the geocoded AVIRIS scene compared with the overlaid forest boundaries (green) and shoreline (blue) of the topographical map. For these subareas, three categories are used to indicate the steepest slope gradient: mild means from flat to a slope angle of about  $15^\circ$ , moderate indicates angles between  $15^\circ$  and about  $30^\circ$ , and steep slope angles with more than  $30^\circ$ . For the discussion, major emphasis is put on the comparison with the scanned forest line because of the improved accuracy and the availability over the whole scene compared with the digitized shoreline.

In general, the results in Figure 7 and Figure 8 show a good correspondence between the geocoded image and the map for all existing topographical locations. In all subareas there are a few locations with minor miscorrespondence between the forest border of the AVIRIS image and the scanned forest line. These problems are almost always restricted to single pixels and no general tendency can be recognized. The error may result from changes in reality between the time the map was published (1987), the used aerial photographs were acquired (1984), and the AVIRIS data are gathered (1991). An additional explanation is based on the fact that maps are always the result of a generalization while AVIRIS displays every occurrence within its resolution characteristics. However, the influence of the cast shadow (of the forest) seems to be not problematic.

Figure 7B demonstrates another problem of the ground reference information, while the lower

regions of the forested slope correspond perfectly the AVIRIS image extends significantly the forest area on the upper limits. This "misregistration" is based on the problem of the determination of the forest border along the timber line and its representation through symbolic point signatures (See chapter "Forest Map").

Figure 7I) and Figure 7E portray areas with rapidly changing slope angle from the lake area to steep slope and from moderate slope to flat area. Figure 10 indicates this phenomena with two profiles. The blue shoreline proves for subarea (D) and the green forest line for subarea (E) the good correspondence.

Figure 8B illustrates the operability of the algorithms in flat and hilly areas. An uncertainty is shown in the lower left forested areas where the map divides the forest with a small street of 4-7m width. Due to the fact that this type of street is usually almost covered with branches of the trees, the AVIRIS pixel can not show this change even despite the big contrast difference in visible bands.

Figures 8D and Figure 8E address an unsolved problem. The comparison of the forested slopes gives good correspondence while the shoreline has an offset between 1 and 3 pixels. Additional investigations at similar locations reject the thesis of an angle dependency between the flight line and the border of the lake for areas with large changes of the slope gradient (compare Fig 7D). A possible explanation may be found due to the fact that the maps have an average paper distortion of about 2.0mm (50m for the map 1:25,000 used in this approach). On the other side, the scanned forested areas are not affected by this problem because they are delivered on high accuracy film. Moreover, the scanned forest mask is geocoded after the scanning process.

### *Quantitative analysis*

The additional verification calculates the average deviation of the geocoded image compared with the forest and lake map. Since this new parametric approach does not use ground control points which could be used for such statistical calculations, an alternative way to achieve a quantitative measure was invented. Both scenes are split into regions consisting of larger and smaller forests. Within each of these regions the largest forest is selected. All points indicating a change in the direction of the forest border line are then considered for measurement of the registration accuracy. At all selected points, the deviation in i and j direction of the DEM is determined. Lines 1 and 2 of Table 2 indicate the results of this test and confirm the visual validation. No systematic deviation was found.

### *Comparison with an improved rubber-sheet approach*

To double-check the performance of the new parametric approach scene Rigi was geocoded using the improved, non-parametric rubber-sheet approach (Itten and Meyer, 1993). For this purpose, out of all checkpoints of the Rigi scene (already defined within the chapter "Quantitative Analysis") those are selected allowing the determination of the deviation. Table 2 (line 3) presents the result for the improved rubber-sheet approach and shows the better performance of the parametric solution. The higher deviations are not surprising since this non-parametric approach can not correct for all flight line and attitude related effects and the influence of the topography on the pixel size.

## **CONCLUSIONS AND OUTLOOK**

The effort of the current investigation was to design and implement a procedure for geocoding Airborne Visible/Infrared Spectrometer (AVIRIS) data in rugged terrain. To correct for the unstable flight line, the attitude movements, and the topographic distortion a parametric approach is presented. The whole procedure is developed to run without human interactions,

The concept of a reconstruction of the geometric situation for every pixel at the time it was acquired proves to work as well in flat and hilly terrain (scene Zug) as in rugged terrain (scene Rigi) for the AVIRIS data. The visual comparison demonstrates good correspondence between the geocoded image and ground reference information. These results are confirmed by an RMS of 0.1 and 0.2 pixel for i and j direction at check points.

The data of the radar tracking system were necessary to achieve a reliable accuracy. Announced improvements of the navigation and engineering data should allow geometric corrections of AVIRIS data independent of external data (Perrin, 1993; Chrien et al., 1993).

The datasets Zug and especially Rigi need georadiometric corrections. Atmospheric corrections using radiative transfer models like MODTRAN-2a (Green et al., 1993) combined with the spectroradiometer measurements of two profiles taken from 50m to 3000m altitude above the lake Zug (scene Zug) and the lake of the Four Cantons (scene Rigi) give hope to correct for the very strong haze layer at 1700m (Staeenz et al., 1993). Corrections for the slope-aspect dependent illumination difference (Meyer et al., 1993a) should finish the preprocessing of the sensor, system and scene related effects of the current data set.

The whole procedure was implemented using the IDL (Interactive Data Language, a proprietary programming language, Research System inc., 1993). The average computational time to correct

a full scene on an IBM RS6000/320H with 32MB RAM is about 25h execution time.

## ACKNOWLEDGMENTS

The author would like to thank the Swiss Research Foundation, Project No. 8220-33290 and the National Aeronautical and Space Administration (NASA) for supporting the project. Thank goes to K. I. Itten, Remote Sensing Laboratory (RSL) at University of Zurich, G. Vane, R. O. Green, and E. G. Hansen, Jet Propulsion Laboratory (JPL) for providing special assistance. The support of the Swiss Air Force is gratefully acknowledged. Thank for extensive cooperation goes to NASA Ames Research Center, High Altitude Flight section and Litton, Acro Products, Woodland Hills, California. The permission to use the digital elevation model (DHM-25), issued by the Swiss Federal Institute of Topography, for this research is greatly appreciated.

Great thank goes to S. A. Larson and E. G. Hansen (JPL), K. I. Itten (RSL) and K. Staenz, Canada Centre for Remote Sensing, Ottawa (CCRS) for the very fruitful discussions and for reviewing.

Thanks for technical assistance go to the staff from the AVIRIS data facility and AVIRIS laboratory (JPL), especially R. O. Green, T. G. Chrien, A. T. Murray, H. I. Novack, M. Solis as well as to T. Kellenberger and E. H. Meier (RSL), and O. Carual (California Institute of Technology).

The results of the comparison between the RC-10 aerial photographs and the ADOUR system are provided by S. Sandmeier (RSL) and are gratefully acknowledged. Thank goes to M. Schaeppman, S. Veraguth, U. Kurer, and D. Schlaepfer (RSL) for geocoding the Rigi scene with the non-parametric approach. The digitizing and scanning of the topographic map, as well as the necessary accuracy investigation were performed by M. Schaeppman and C. Ehrler (RSL).

The work described in this paper was carried out at the Jet Propulsion Laboratory, California Institute of Technology.

## REFERENCES

- Chrien, T.G., Eastwood, M. L., Sarture, C. M., Green, R. O. (1993), AVIRIS instrument status, in *Proc. of the Fourth Geoscience Workshop* (in preparation).
- Ferraro, R. F., (1988), Programmer's Guide to the EGA and VGA Cards, Addison-Wesley Publishing Company Inc., Reading, pp. 165-167.
- Frey, F., Bischof, A. Meyer, P., Itten, K. I., and Staenz, K. (1989), Preprocessing of Airborne Multi-spectral Scanner data for forest damage assessment in hilly terrain, in *Proc. of the IGARSS'89 Symposium*, Vancouver, BC, pp. 2374-2377.
- Genofsky, J.J. (1886), Earths' rotational effects on the AVIRIS Gyro, JPL Interoffice Memorandum AVIRIS-DF# 097, Pasadena, CA, p. 4.
- Green, R. (). Conel, J. E., T. G. Chrien (1993), Correction of AVIRIS radiance to reflectance using MODTRAN-2, in *Proc. International Society for Optical Engineering (SPIE) 1937*, Orlando, FL (in press).
- Guindon, B. (1980), Integration of MSS and SAR data of forested regions in mountainous terrain, in *Proc. of the 14(th) International Symposium on Remote Sensing*, Winnipeg, Ca, pp. 1673-1690.
- Horn, R., Moreira, J., Meier E. H., Piesbergen, J., Cocard, M. M., and Hounam, D. (1993), A refined procedure to generate calibrated imagery from Airborne Synthetic Aperture Radar Data, *IEEE Transactions on Geoscience and Remote Sensing* (submitted).
- Itten, K. I., and Meyer, P (1993), Georadiometric correction of TM-Data of mountainous forest areas, *IEEE Transactions on Geoscience and Remote Sensing* (in press).
- Itten, K. I., Meyer, P., Staenz, K., Kellenberger, T., and Schaepman, M. (1992), Evaluation of the AVIRISwiss'91 campaign data, in *Proc. of the 7'bird Geoscience Workshop*, JPL Pub]. 92,-14, Vol 1, Jet Propulsion Laboratory, Pasadena CA, pp. 108-110.
- Kalcic, M. T., and Lingsch, S. C. (1991), Multispectral software development for the Airborne Bathymetric Survey System, Naval Oceanographic and Atmospheric Research Laboratory NOARI Report 17, p. 9.
- Larson, S., Meyer, P., and Hansen, E. G. (1994), Topographical and geometric correction of remote sensing image data using dead reckoning, *IEEE Transactions on Geoscience and Remote Sensing* (in preparation).
- Litton System Inc. (1989), Fundamentals of strapdown inertial navigation, Document No. 406372, Woodland Hills, CA.
- Meyer, P., and Itten, K. I. (1992), Datenbankbasierte Klassifikation eines Multispektralscanner-Datensatz, *Zeitschrift für Photogrammetrie und Fernerkundung*, 5/92: 149-158.
- Meyer, P., (1992), Segmentation and symbolic description for a classification of agricultural areas with multispectral scanner data, *IEEE Transaction on Geoscience and Remote Sensing*, Vol. 30, 5:673-679.
- Meyer, P. Itten, K. I., Kellenberger, T., Leu, R., and Sandmeier, S. (1993a), Radiometric and Geometric Correction of TM-Data of Mountainous Forest Areas, *ISPRS Journal Photogrammetric Engineering and Remote Sensing/Photogrammetria* (in press).
- Meyer, P., Green, R. O., and Chrien, T. G. (1993b), Spectral, radiometric, and geometric quality assessment of AVIRIS data, in *Proc. of the Fourth Geoscience Workshop* (in preparation).
- Perrin, D. (1993), Personal communication (fax Jan 28, 1993)
- Rickenbacher, M. (1992), Das digitale Höhenmodell DHM25 und seine möglichen Anwendungen in der amtlichen Vermessung, *Journal Vermessung, Photogrammetrie und Kulturtechnik, VPK*, No. 12/92.
- Research Systems, Inc<sup>®</sup>. (1993), IDL User's Guide, Version 3.0, Boulder, CO.

- Staenz, K., Teillet, P. M., Meyer, P., Williams, J. J., and Itten, K. I. (1993), Low-altitude radiance measurements in support of surface reflectance retrieval from AVIRIS Data, in *Proc. 25th International Symposium on Remote Sensing and Global Environmental Change*, ERIM, Graz, Austria (in press).
- The Singer Company (1984), Kearfott Conax Gyros, FSCM No. 88818, Little Falls, NJ.
- Thomson-CSF (1987), Radar ADOUR, Modernisation télémétrie et codage, Tome I.
- Vane, G., Green, R. O., Chrien, T. G., Enmark, H. T., Hansen, E. G., and Porter, W. M. (1993), The Airborne Visible/Infrared imaging Spectrometer (AVIRIS), *Remote Sens. Environ.* 44: 127-143.

Figure 1: Regression y for the difference in altitude z between the projection center (PC) of the RC-10 aerial photographs and the corresponding values of the ADOUR Conical Radar Tracking System.

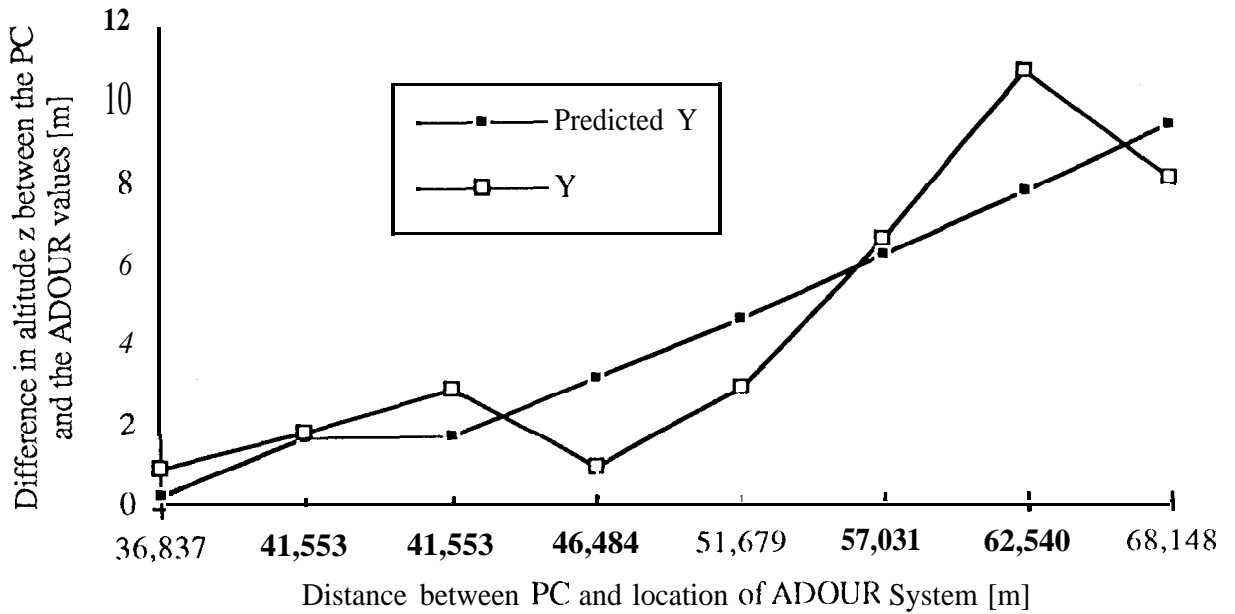


Figure 2: Overview of the data preparation and core tasks of the geocoding approach, where  $x$ =latitude,  $y$ =longitude,  $z$ =altitude of the airplane, and  $c$ =column and  $r$ =row of the raw file.

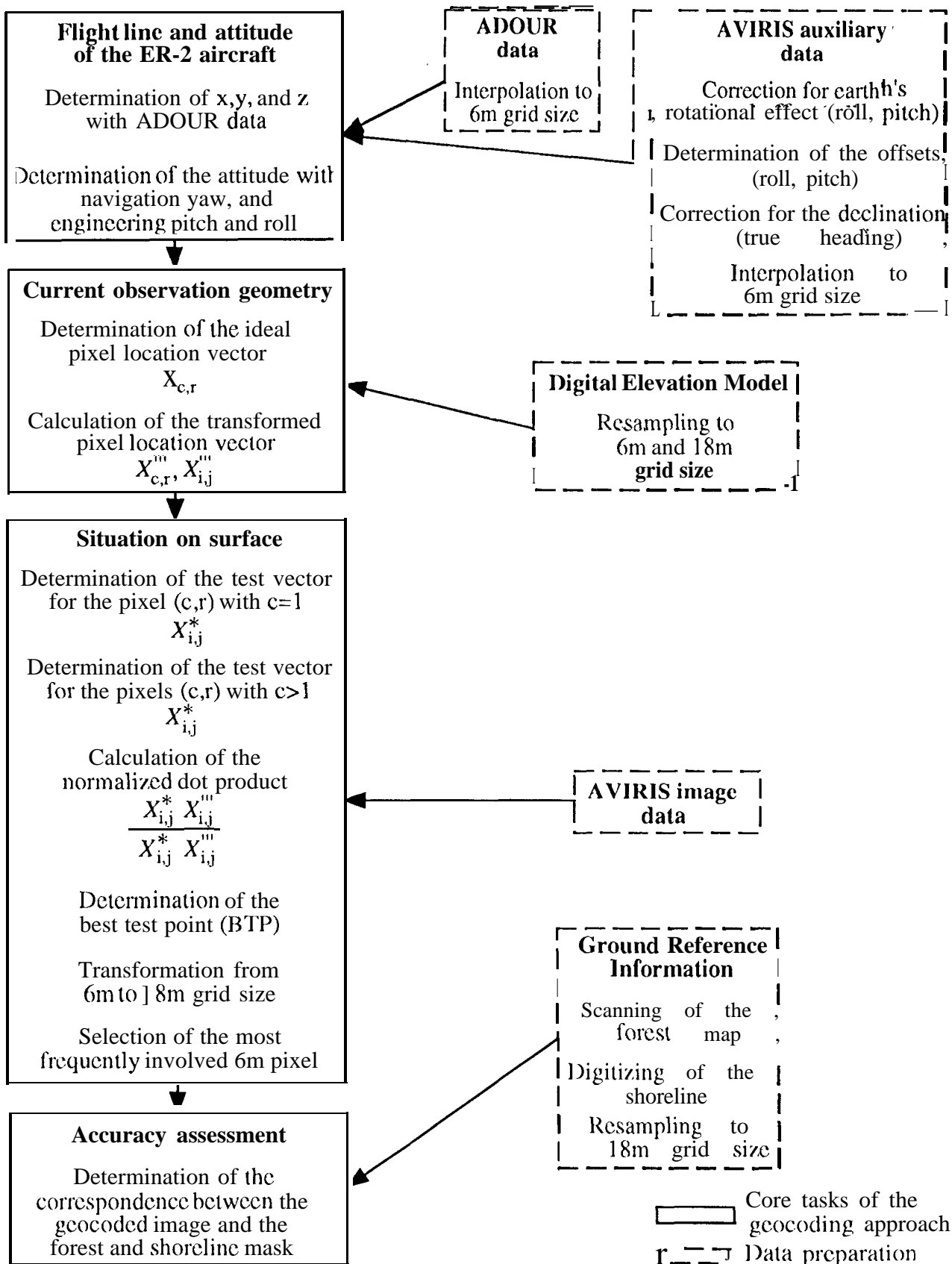
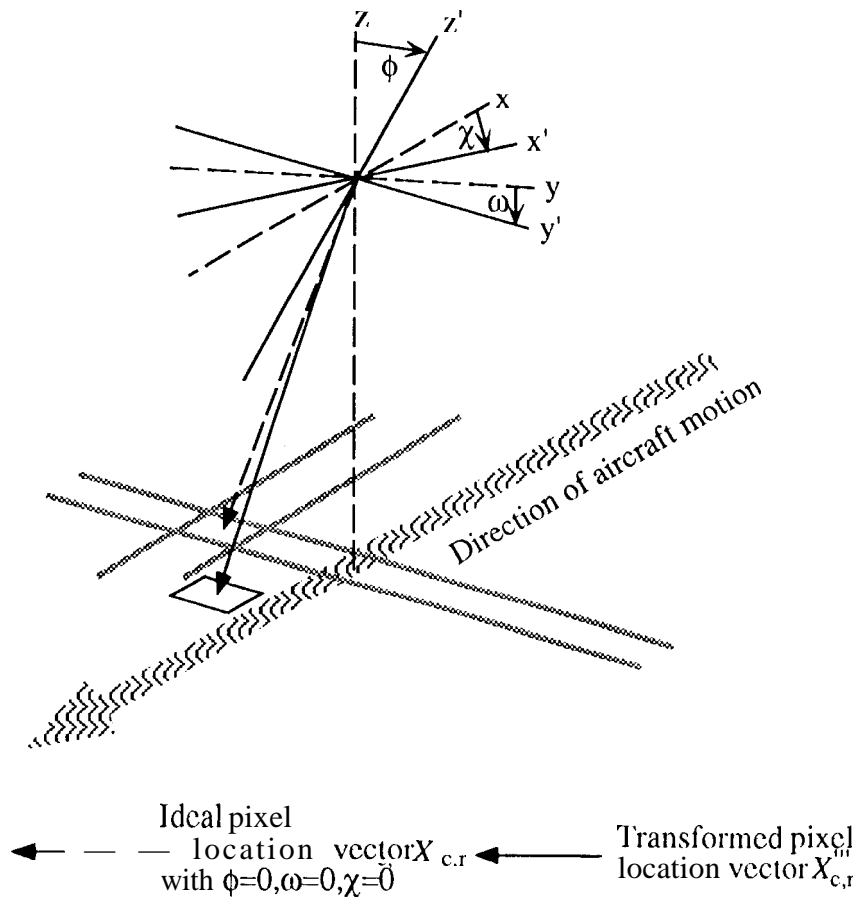
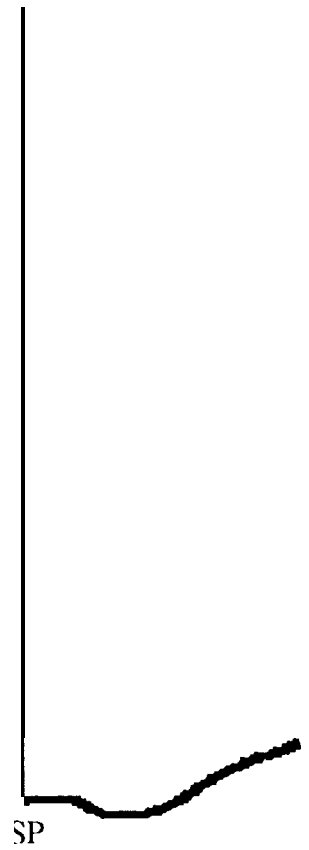


Figure 3: Principle outline of the observation geometry to calculate the transformed pixel location vector where  $\phi$ =pitch,  $\omega$ =roll, and  $\chi$ =true heading, and  $x,y,z$  defining the coordinate axis for the ideal pixel location vector and  $x',y',z'$  for the transformed pixel location vector.



Aircraft



← Test vector  $X_{c,r}^*$

Figure 5: Situation on surface for the test vectors for pixel (c,r) with  $c > 1$ , where BTpP=best test point for previous pixel (c-1,r), and BTP=best test point for current pixel (c,r) with  $c > 1$ .

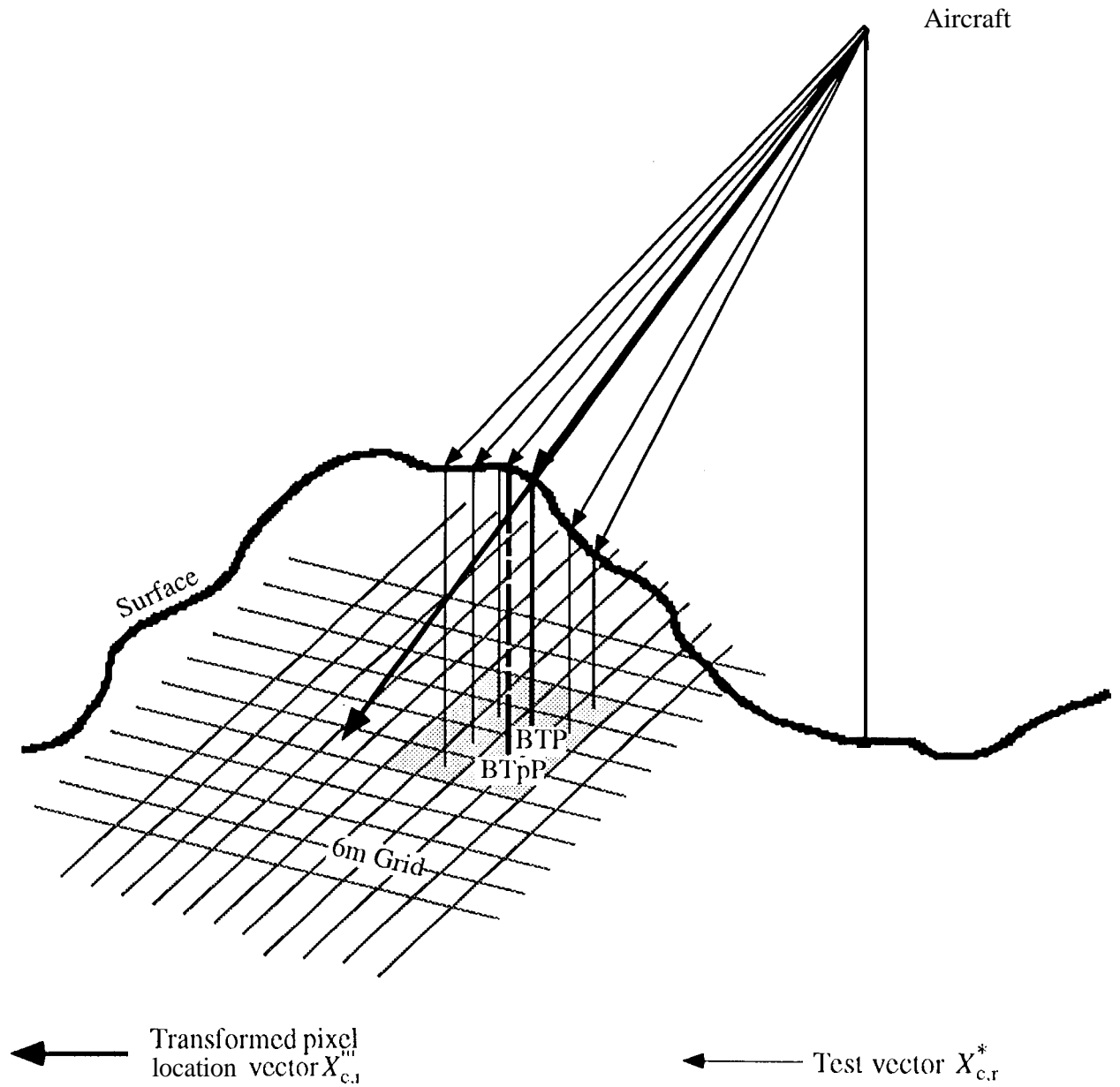
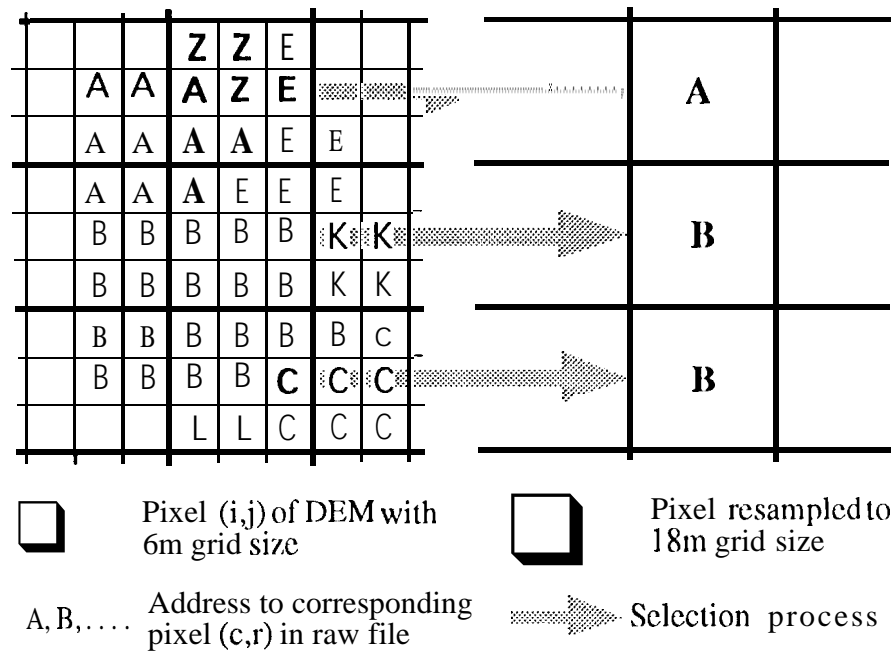


Figure 6: Procedure to define the Digital Number (DN) of the new resampled pixel with 18m grid size. Within the area of the 18m pixel, the most frequent 6m pixel (i,j) is determined. The address of this pixel points to the corresponding pixel (c,r) in the raw file. The DN of this corresponding pixel becomes the DN of the geocoded, resampled 18m pixel.





A) Overview



B) North, steep slope



C) Northwest, moderate slope

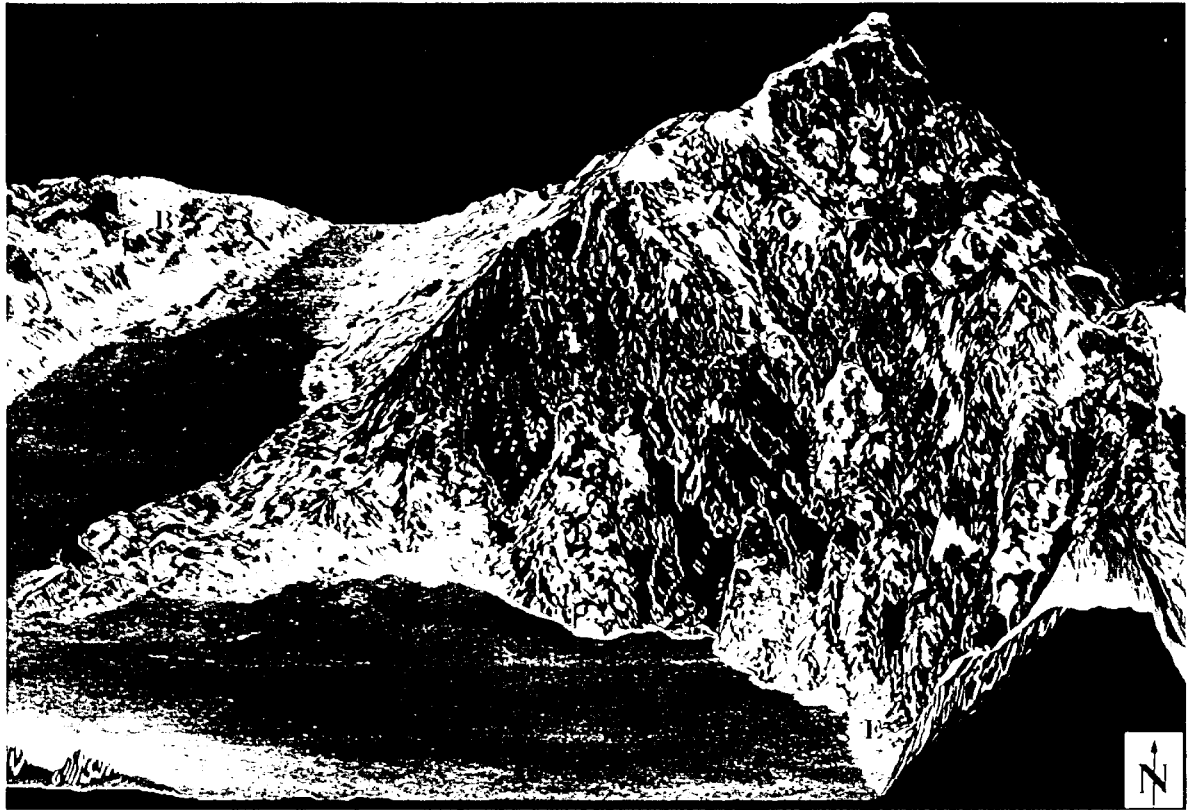


D) Northeast, steep slope



E) Northwest, 1110° (1.1°) slope

Figure 7: Northern part of the scene Rigi: Bands 13, 18, and 28 of the geocoded image are overlaid by the scanned forest (green line) and the digitized shoreline (blue line). (A) shows the composite rendered 011 the digital elevation model with lags (11-1; for the location of the enlarged subareas of the horizontal (non-rendered) composite. (B)-(E) show zoom-up ( $\approx$  factor 5) parts with different aspect and slope angles. CS1 indicates the starting point for north-south cross-section and CS2 for the west-east shown in Figure 9



A) Overview



B) Southeast, mild slope



C) Northeast and Southwest (valley), steep slope



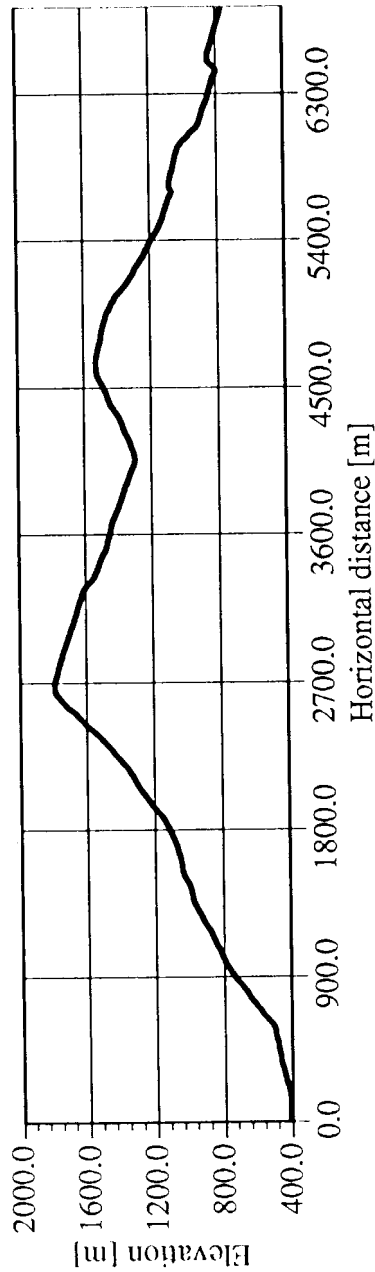
D) South, steep slope



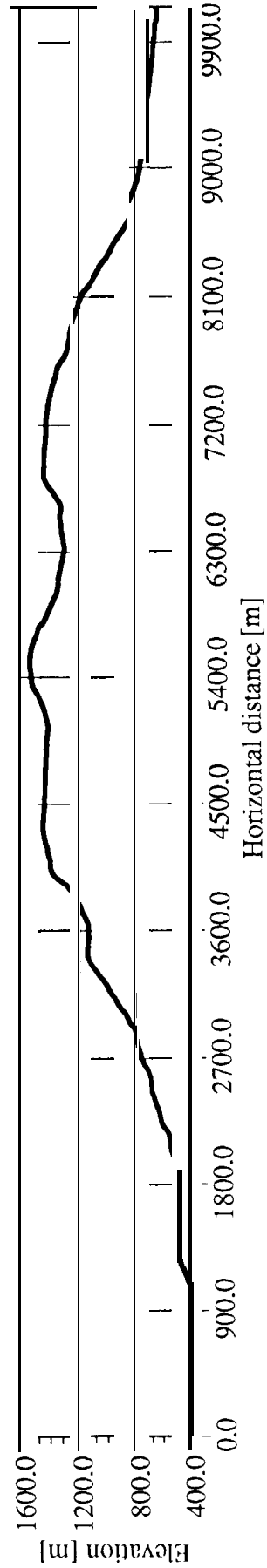
E) West, steep slope

Figure 8: Southern part of the scene Rigi; Bands 13, 18, and 28 of the geocoded image overlaid by the scanned forest (green line) and the digitized shoreline (blue line). (A) shows the composite rendered on the digital elevation model with tags (B-E) for the location of the enlarged subareas of the horizontal (non-rendered) composite. (B)-(E) show zoom-up ( $\approx$  factor 5) parts with different aspect and slope angles.

Figure 9: '1'-scale cross-section for the scene Rigi. (A) shows the north-south profile (CS 1), and (B) the west-east (CS2) at the location indicated in Fig. 7.

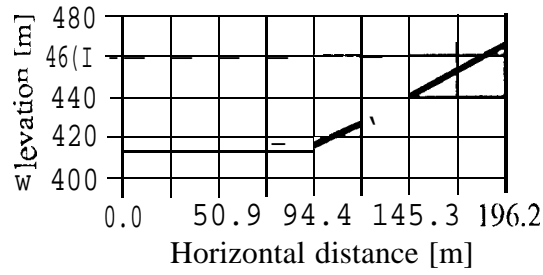


(A) North-south cross-section (CS1)

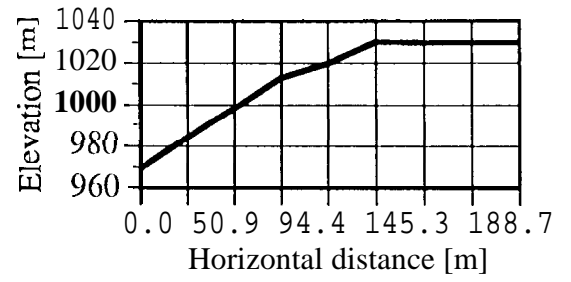


(B) West-east cross-section (CS2)

Figure 10: To-scale cross section to show the rapid terrain change. (A) shows the change from the lake to the slope at the foot of the mountain Rigi for the subarea of Figure 7D while (B) demonstrates the change from a moderate slope to flat terrain for the subarea of Figure 7E.



(A)



(B)

## Tables

Table 1: Accuracy assessment for the ADOUR Conical Radar Tracking System with a comparison of the absolute pointing measurements between the two devices (upper line) and the projection center (PC) of the RC-10 aerial photographs and the measurements of the device 1 (lower line).

	<i>Longitude y mean (RMS) [m]</i>	<i>Latitude x mean (RMS) [m]</i>	<i>Altitude z mean (RMS) [m]</i>
Distance between device 1 and device 2	1.08 (6.36)	6.29 (8.20)	1.51 (5.24)
Distance between PC and device 1	1.22 (21.70)	30.51 (23.32)	2.00 (5.50)

Table 2: Result of the quantitative effort for the comparison between the geocoded images and the forest map with the RMS for the east-west direction (i) and north-south direction (j) of the digital elevation model. The check points used for the non-parametric approach for scene Rigi are a selection from the entire member of points used for the parametric approach.

	<i>Number of RMS for i-direction checkpoints</i>	<i>RMS for i-direction [pixels]</i>	<i>RMS for j-direction [pixels]</i>
Scene Zug (parametric approach)	186	0.07	0.19
Scene Rigi (parametric approach)	309	0.12	0.09
Scene Rigi (non-parametric approach)	249	3.57	1.37